

The effect of compositional change of transition metals on the electrochemical behavior of layered LiMO_2 ($M = \text{Li}_w\text{Ni}_x\text{Co}_y\text{Mn}_z$) solid solutions

Sung Jang Jin^a, Chi Hoon Song^a, Ki Soo Park^a, A. Manuel Stephan^a,
Kee Suk Nahm^{a,*}, Yun Sung Lee^b, Jae Kook Kim^c, Hoon Taek Chung^d

^a School of Chemical Engineering and Technology, Chonbuk National University, Jeonju 561-756, Republic of Korea

^b Faculty of Applied Chemical Engineering, Chonnam University, Kwangju 500-757, South Korea

^c Department of Materials Science and Engineering, Chonnam University, Kwangju 500-757, South Korea

^d Department of Ceramic Engineering, Dong-Shin University, 252 Naju, Chonnam 520-714, South Korea

Received 18 August 2005; received in revised form 4 October 2005; accepted 4 October 2005

Available online 5 December 2005

Abstract

Seven compositions of LiMO_2 ($M = \text{Li}_w\text{Ni}_x\text{Co}_y\text{Mn}_z$) ($w = 1/15 - 1/6$; $x = 0 - 3/10$; $y = 1/5 - 1/2$; $z = 13/30 - 1/3$; i.e. $w + x + y + z = 1$) solid solutions were synthesized using the sol–gel method with the following end members LiCoO_2 , Li_2MnO_3 ($\text{Li}[\text{Li}_{1/3}\text{Mn}_{2/3}]\text{O}_2$), and $\text{Li}[\text{Ni}_{0.5}\text{Mn}_{0.5}]\text{O}_2$. The electrochemical behavior of the solid solutions was analyzed for the various compositions of metals in transition metal sites. All synthesized particles were semi-spherically shaped with a layered structure. When the content of lithium and cobalt was reduced (while the other metals were increased), the lattice parameters, a and c , decreased and were accompanied by a shift in the Raman spectrum. The cycling studies reveal that the compound, $\text{Li}[\text{Li}_{1/12}\text{Ni}_{1/4}\text{Co}_{1/4}\text{Mn}_{5/12}]\text{O}_2$ was found to be optimal in voltage and from a stability point of view.
© 2005 Elsevier B.V. All rights reserved.

Keywords: Lithium battery; Cathode material; Sol–gel method; Solid solution; Layered structure

1. Introduction

Currently, LiCoO_2 is the most widely commercialized cathode material for the lithium secondary batteries due to its ease of preparation, acceptable specific capacity, high rate capability and long cycle life. In the recent years, in order to preserve the electrochemical properties of cobalt and nickel and thermal properties of manganese, compounds like $\text{LiNi}_{0.8}\text{Co}_{0.2}\text{O}_2$ and $\text{LiNi}_{1/2-y/2}\text{Mn}_{1/2-y/2}\text{Co}_y\text{O}_2$ have drawn the attention of many researchers [1,2]. The preparation of solid solutions with layered manganese oxides has been extensively studied because of its stable structure and good electrochemical performance.

Ohzuku et al. [3] reported the cycling behavior of $\text{LiNi}_{0.5}\text{Mn}_{0.5}\text{O}_2$ between the 2.5 and 4.3 V which delivered a discharge capacity of 150 mAh g^{-1} . Kang et al. [4] have synthe-

sized a solid solution with two end members of Li_2MnO_3 and $\text{Li}[\text{Ni}_{0.5}\text{Mn}_{0.5}]\text{O}_2$ with a mixing ratio of 1:1. They reported that the $0.5\text{Li}[\text{Ni}_{0.5}\text{Mn}_{0.5}]\text{O}_2-0.5\text{Li}[\text{Li}_{1/3}\text{Mn}_{2/3}]\text{O}_2$ solid mixture formed a layered structure solid solution with a gradual increase in the discharge capacity from 170 to 210 mAh g^{-1} in the voltage region 2.0–4.6 V. Although, Li_2MnO_3 ($\text{Li}[\text{Li}_{1/3}\text{Mn}_{2/3}]\text{O}_2$) is electrochemically inactive the solid solution with Li_2MnO_3 ($\text{Li}[\text{Li}_{1/3}\text{Mn}_{2/3}]\text{O}_2$) as the end member showed a gradual increase of discharge capacity from the first cycle [5,6]. Numata et al. [7] reported the electrochemical properties of $\text{Li}(\text{Co}_{1-x}\text{Li}_x\text{Mn}_{2x/3})\text{O}_2$ solid solutions with two end members, LiCoO_2 and Li_2MnO_3 . The authors also observed that the electrochemical properties of the solid solutions had been considerably reduced when the content of Li_2MnO_3 was increased in the compound. In a similar study, Kim et al. [8] and Zhang et al. [9] synthesized solid solutions with layered manganese oxides using three end members: LiCoO_2 , Li_2MnO_3 , and $\text{Li}[\text{Ni}_{0.5}\text{Mn}_{0.5}]\text{O}_2$, and found that these solid solution produced better electrochemical properties than LiCoO_2 . They examined the effect of Co

* Corresponding author. Tel.: +82 63 270 2311; fax: +82 63 270 2306.
E-mail address: nahmks@chonbuk.ac.kr (K.S. Nahm).

content in the materials by changing the mixing ratio of the two end members including LiCoO₂. Kim et al. [8] fixed the composition of Li₂MnO₃ at 0.3, and changed the mixing ratio of LiCoO₂ in 0.7(LiCoO₂ + Li[Li_{0.5}Mn_{0.5}O₂]). While increasing the LiCoO₂ composition, the layer-like structure of the synthesized materials were enhanced and exhibited a low resistance value on cycling. On the other hand, Zhang et al. [9] changed the mixing ratio of LiCoO₂ in 0.4(LiCoO₂ + Li₂MnO₃), while maintaining 0.6Li[Ni_{0.5}Mn_{0.5}O₂]. They observed an increase in the value of the discharge capacity when the composition of LiCoO₂ was reduced. Further, to investigate the effect of metal composition in the transition metal layers, they fixed one end member concentration, while changing the compositions of other two end members. In the present work, layered manganese oxides solid solutions of LiMO₂ (M = Li_wNi_xCo_yMn_z) ($w = 1/15 - 1/6; x = 0 - 3/10; y = 1/5 - 1/2; z = 13/30 - 1/3$; i.e. $w + x + y + z = 1$) were synthesized with three end members: LiCoO₂, Li₂MnO₃(Li[Li_{1/3}Mn_{2/3}O₂]), and Li[Ni_{0.5}Mn_{0.5}O₂] using a sol–gel method. In order to understand the influence of the metals on the structural and electrochemical properties of the solid solutions, the compositions of metals in transition metal sites were adjusted by changing the mixing ratio of the three end members which are discussed below.

2. Experimental

LiMO₂ (M = Li_wNi_xCo_yMn_z) ($w = 1/15 - 1/6; x = 0 - 3/10; y = 1/5 - 1/2; z = 13/30 - 1/3$; i.e. $w + x + y + z = 1$) compounds were prepared by a sol–gel method using glycolic acid as a chelating agent. Stoichiometric amounts of CH₃COOLi·2H₂O (Kanto), (CH₃COO)₂Ni·4H₂O (Aldrich), (CH₃COO)₂Co·4H₂O (Aldrich), and (CH₃COO)₂Mn·4H₂O (Acros) were dissolved in DI water. The dissolved solution was added drop by drop to the continuously agitated aqueous solution with glycolic acid. The pH of the solution was in the range of 5–5.5. The prepared solution was evaporated at 70–80 °C. The resulting precursors were heated at a ramping rate of 1 °C min⁻¹ and decomposed at 450 °C for 10 h in air. Then, the decomposed powders were calcined for 10 h at 950 °C and quenched to room temperature. Provided in Table 1 is the information on the samples synthesized and the summarized results of Rietveld refinements from their XRD spectra.

The powder X-ray diffraction (XRD, D/Max 2500, Rigaku) measurement using Cu K α radiation was employed to charac-

terize the crystalline phase of the synthesized material. Rietveld refinement (Fullprof 2000, LLB) was performed on the X-ray diffraction data to identify the variation of constants for the unit cell. The crystal structure of the synthesized material was also confirmed by a micro-Raman spectrometer (RS spectra, RS 100, Reinsho) with holographic gratings. The laser light source was the 514 nm line radiation from a Spectra-Physics 2020 argon ion laser. The morphology of the prepared material was observed by field emission scanning electron microscope (FE-SEM, S-4700, Hitach).

The electrochemical characterization was carried out using a 2032-type coin cell (Hosen). For the fabrication of the cathode, 20 mg of prepared LiMO₂ (M = Li_wNi_xCo_yMn_z) ($w = 1/15 - 1/6; x = 0 - 3/10; y = 1/5 - 1/2; z = 13/30 - 1/3$; i.e. $w + x + y + z = 1$) compounds were mixed with 12 mg of conductive binder (8 mg of teflonized acetylene black and 4 mg of graphite). The mixture was pressed onto 20 mm² stainless steel mesh, which was used as the current collector, and dried at 100 °C for 10 h in a vacuum oven. The cells were comprised: of the cathode and the lithium foil (Cyprus Foote Mineral) anode, separated by a porous polypropylene film separator (Celgard 3401). The electrolyte was a 1 M LiPF₆—ethylene carbonate (EC)/dimethyl carbonate (DMC) at a 1:2 volume ratio (Merck). The cells were assembled in an argon-filled dry box and tested at room temperature. The cells were charged and discharged at a current density of 0.4 mA cm⁻² in the voltage range: 2.5–4.5 V.

3. Results and discussion

3.1. SEM analysis

Fig. 1a–g shows the FE-SEM images of the prepared samples of LiMO₂ (M = Li_wNi_xCo_yMn_z) (the compositions of the samples are denoted as A–G as displayed in Table 1). The particles seem to be semi-spherically shaped and are agglomerated. The average sizes of the particles are found to be between 250 and 500 nm.

3.2. X-ray diffraction studies

Fig. 2 shows the XRD patterns of the prepared LiMO₂ samples with their corresponding Miller indices. The XRD peaks are all indexed based on a hexagonal α -NaFeO₂ structure with the space group $R\bar{3}m$ (S.G. no. 166), except that the super lattice ordering peaks between 20 and 25° as shown in dotted rect-

Table 1

The compositions of LiMO₂ (M = Li_wNi_xCo_yMn_z) prepared and the results of Rietveld refinements on XRD spectra of the materials

Sample name	x	Composition	a (Å)	c (Å)	cla	R _p (%)	R _{wp} (%)	R _{exp} (%)
A	0.0	Li[Li _{1/6} Co _{1/2} Mn _{1/3}]O ₂	2.8646	14.2512	4.9748	14.3	17.7	7.32
B	0.1	Li[Li _{3/20} Ni _{1/20} Co _{9/20} Mn _{7/20}]O ₂	2.8582	14.2365	4.9810	13.8	16.7	7.02
C	0.2	Li[Li _{2/15} Ni _{1/10} Co _{2/5} Mn _{11/30}]O ₂	2.8545	14.2320	4.9859	13.1	16.0	6.75
D	0.3	Li[Li _{7/60} Ni _{3/20} Co _{7/20} Mn _{23/60}]O ₂	2.8311	14.1682	5.0045	12.7	14.9	6.55
E	0.4	Li[Li _{1/10} Ni _{1/5} Co _{3/10} Mn _{2/5}]O ₂	2.8419	14.2042	4.9982	11.1	13.9	6.32
F	0.5	Li[Li _{1/12} Ni _{1/4} Co _{1/4} Mn _{5/12}]O ₂	2.8459	14.2089	4.9929	10.8	13.1	6.24
G	0.6	Li _{1/15} Ni _{3/10} Co _{1/5} Mn _{13/30}]O ₂	2.8245	14.1514	5.0102	9.9	12.6	6.02

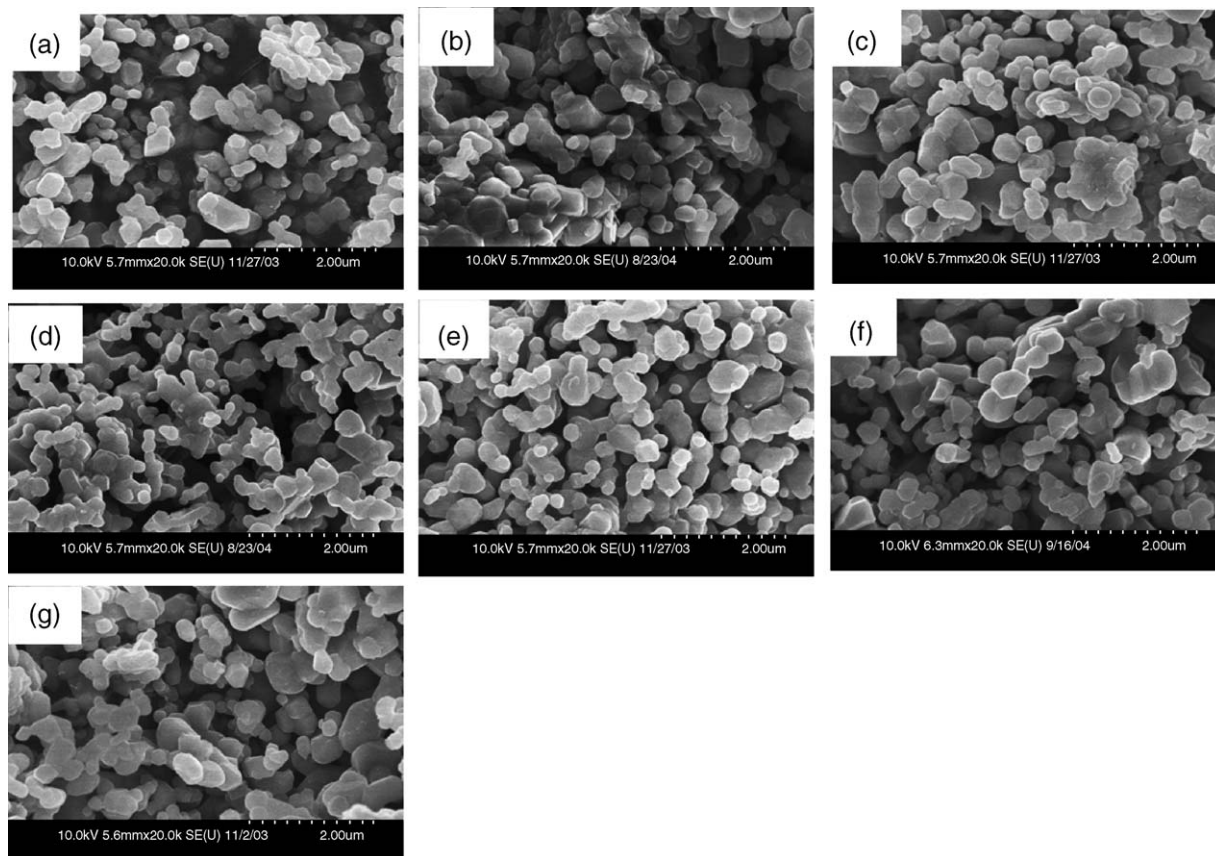


Fig. 1. FE-SEM photographs of the LiMO_2 ($M = \text{Li}_w\text{Ni}_x\text{Co}_y\text{Mn}_z$) powders.

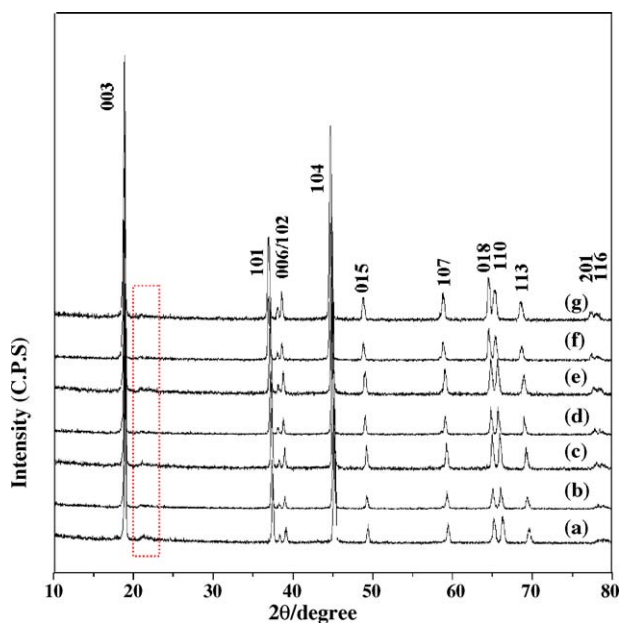


Fig. 2. X-ray diffraction patterns of the LiMO_2 ($M = \text{Li}_w\text{Ni}_x\text{Co}_y\text{Mn}_z$) powders.

angle. The peak observed from the samples A–G results from short range ordering of Li, Co, Ni and Mn atoms in the transition metal layers, indicating a characteristic feature of Li_2MnO_3 structure [10]. Recently, Grey et al. [11] reported the ordering

of Li_2MnO_3 – $\text{Li}[\text{Ni}_{0.5}\text{Mn}_{0.5}]\text{O}_2$. Li-NMR was used as a tool to analyze these compounds and the authors found that the layers of $[\text{Li}_{1/3}\text{Mn}_{2/3}]$ in Li_2MnO_3 are well ordered. Also, the same authors proved [12] that the Li_2MO_3 ($M = \text{Ti}, \text{Mn}, \text{Zr}$) component is structurally integrated into the $\text{LiMn}_{0.5}\text{Ni}_{0.5}\text{O}_2$ component and yields composite structures with domains having short range order and are not in the form of true solid solutions, in which the cations are uniformly distributed within the discrete layers. But these results are in contradiction to those reported by Dahn et al. [13]. Hence, it appears that as a general consensus these materials have extremely complex structures with inhomogeneous cation distributions. The calculated lattice parameters, a , c and c/a ratio, using the Rietveld refinement for XRD data for the samples A–G are listed in Table 1. The values of a and c decrease when the contents of Mn and Ni are increased. The decrease in the values of the lattice parameter is attributed to the substituted Ni^{2+} ($r_{\text{Ni}^{2+}} = 0.69 \text{ \AA}$) and Mn^{4+} ($r_{\text{Mn}^{4+}} = 0.53 \text{ \AA}$) ions which are smaller than Li^+ ($r_{\text{Li}^+} = 0.76 \text{ \AA}$) and Co^{3+} ($r_{\text{Co}^{3+}} = 0.545 \text{ \AA}$) ions in size. The changes of the lattice parameters obey Vegard's law and these results are in accordance with earlier reports [5,6]. The c/a ratio of the samples is >4.9 , which suggests that the prepared samples have a layered structure with hexagonal crystals. Although, super lattice ordering peaks exist, the clear splitting of the peaks assigned to the Miller indices (006, 102) and (108, 110) indicate that the synthesized samples have a typical layered structure.

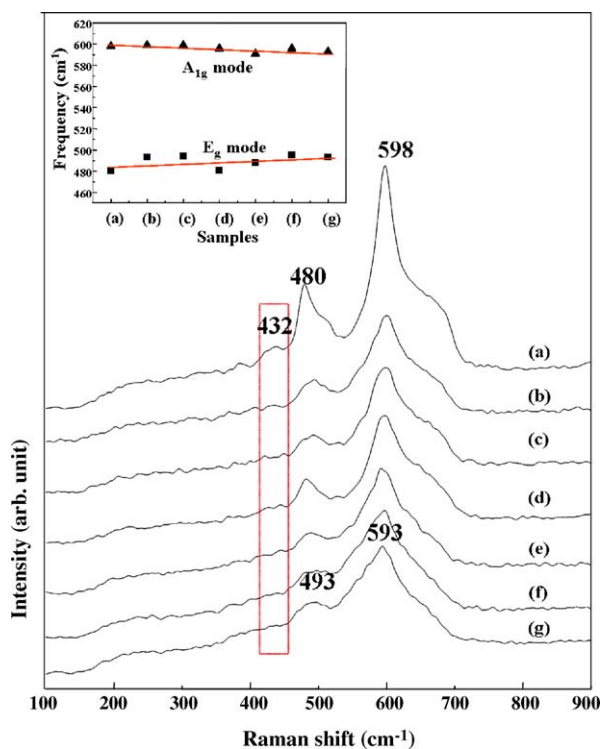


Fig. 3. Raman spectra of the LiMO_2 ($M = \text{Li}_w\text{Ni}_x\text{Co}_y\text{Mn}_z$) powders. The inset shows the frequency shift of the Raman modes for each sample.

3.3. Raman spectra analysis

In order to substantiate the XRD data, the Raman spectra have been used as a complementary tool in the recent years [14–17]. Fig. 3a–g displays the Raman spectra of the samples prepared for the various lithium contents. It is quite obvious from the Fig. 3, that the peak which starts around 575 cm^{-1} is sharpened when the content of lithium is increased. The intensity of the peak was found to be a maximum when the content of lithium is high. This increase of intensity with the increase of lithium content is attributed to the decrease of electrostatic repulsion between adjacent layers of the compound. Also, the negatively charged oxygen–oxygen interaction decreases, when the content of lithium is increased. The observed upward shift of the bands is attributed to a contraction of the c -axis direction [17–19]. These results are in accordance with the lattice parameter values as depicted in Table 1. A similar observation was observed by Wu et al. [17] in which the authors reported the Raman and XRD analysis for $\text{Li}_{2.26}\text{Mn}_{0.91}\text{Cr}_{1.29}\text{O}_{4.93}$, $\text{Li}_{2.70}\text{Mn}_{0.91}\text{Cr}_{1.08}\text{O}_{5.13}$ and $\text{Li}_{3.07}\text{Mn}_{0.91}\text{Cr}_{1.06}\text{O}_{5.37}$.

3.4. Charge–discharge studies

Fig. 4 shows the capacity versus voltage profiles of the fabricated Li/LiMO_2 ($M = \text{Li}_w\text{Ni}_x\text{Co}_y\text{Mn}_z$) cells at 25°C . All the samples exhibit smooth and monotonous charge/discharge curves, which are normally observed with the typical layered solid solutions for manganese oxides [20], which substantiates, that our prepared samples have a layered structure. The

cycling behavior of the samples A–D was different from that of the samples E–G. The discharge capacity of the samples A–D increased initially and a fade in capacity was observed upon further cycling. On the other hand, samples E–G, exhibited capacity fading from the first cycle. This type of electrochemical behavior has generally been observed from manganese oxide solid solutions with Li ions in the transition metal sites and is attributed to the structural formation without transition to the spinel structure [5,6]. The charge–discharge behavior of the sample G is very similar to the cycling characteristics of typical LiNiO_2 [21]. Nonetheless, the capacity of the samples E–G slightly decreases upon cycling, the fade in capacity per cycle is very low and the enhanced cyclability can be believed due to the presence of $\text{Mn}^{3+}/\text{Mn}^{4+}$ and $\text{Ni}^{4+}/\text{Ni}^{2+}$ couples. Among the samples studied, the compound F, $\text{Li}[(\text{CoLi}_{1/3}\text{Mn}_{2/3})_{(1-x)/2}(\text{Ni}_{1/2}\text{Mn}_{1/2})_x]\text{O}_2$ ($x = 0.5$) exhibits a stable voltage profile.

Fig. 5 shows the plots of discharge capacity versus cycle number of the Li/LiMO_2 cells. In the first cycle, the discharge capacities of the samples A–G were 169, 185, 172, 165, 167, 170 and 170 mAh g^{-1} , respectively. The samples A–D showed an initial increase of the discharge capacity up to a few cycles and the samples E–G exhibited a decrease in the discharge capacity from the first cycle. The discharge capacity of sample A is 169 mAh g^{-1} in the first cycle and then gradually increases to a maximum of 198 mAh g^{-1} in the sixth cycle. A similar trend was observed for other samples B–D. The samples A–D delivered an initial discharge capacity of 169, 185, 172 and 165 mAh g^{-1} during the first cycle and 178, 195, 178 and 165 mAh g^{-1} at the end of 50th cycle. Upon cycling (50 cycles) we could not observe any fade in capacity for the samples A–D. On the other hand, the samples E–G exhibited a slight fade in capacity of 0.16, 0.04 and 0.20 mAh g^{-1} per cycle, respectively. A fade in capacity upon cycling for layered manganese oxide compounds has been observed by many researchers [22–24]. They observed an initial increase in the discharge capacity with the cycle number and after reaching the maximum value it underwent capacity fading. According to Kim et al. [25], this phenomenon occurs due to the stabilization of synthesized solid solutions with cycling. The rate of lithium insertion and extraction at a high current density is very fast and the manganese oxides are progressively stabilized in the structure with cycling. They also reported that the increase in the initial discharge capacity is due to the oxidation state of Mn which varies from 4+ to 3+ (discharging process) or from 3+ to 4+ (charging process) during cycling. Samples E–G exhibited minimum capacity fading even after the 50th cycle. The discharge capacity and fade in capacity per cycle are shown in an inserted table in Fig. 5.

The composition of metals in transition metal sites changes in the following order for the samples A–G, i.e. the compositions of Li and Co decrease, whereas those of Mn and Ni increase. It seems that the discharge capacity of the sample A is influenced mainly by the $\text{Co}^{3+}/\text{Co}^{4+}$ and $\text{Mn}^{3+}/\text{Mn}^{4+}$ couples with a mixing ratio of the end members: LiCoO_2 and Li_2MnO_3 , $\text{Li}[(\text{CoLi}_{1/3}\text{Mn}_{2/3})_{(1-x)/2}(\text{Ni}_{1/2}\text{Mn}_{1/2})_x]\text{O}_2$ 0.5:0.5, when $x = 0$. Fig. 6a shows the plot of dQ/dV versus voltage for the sample A. The main peaks appearing around 3.8 V are due to the $\text{Co}^{3+}/\text{Co}^{4+}$ redox couple and the broad peaks at 3.4–3.5 V

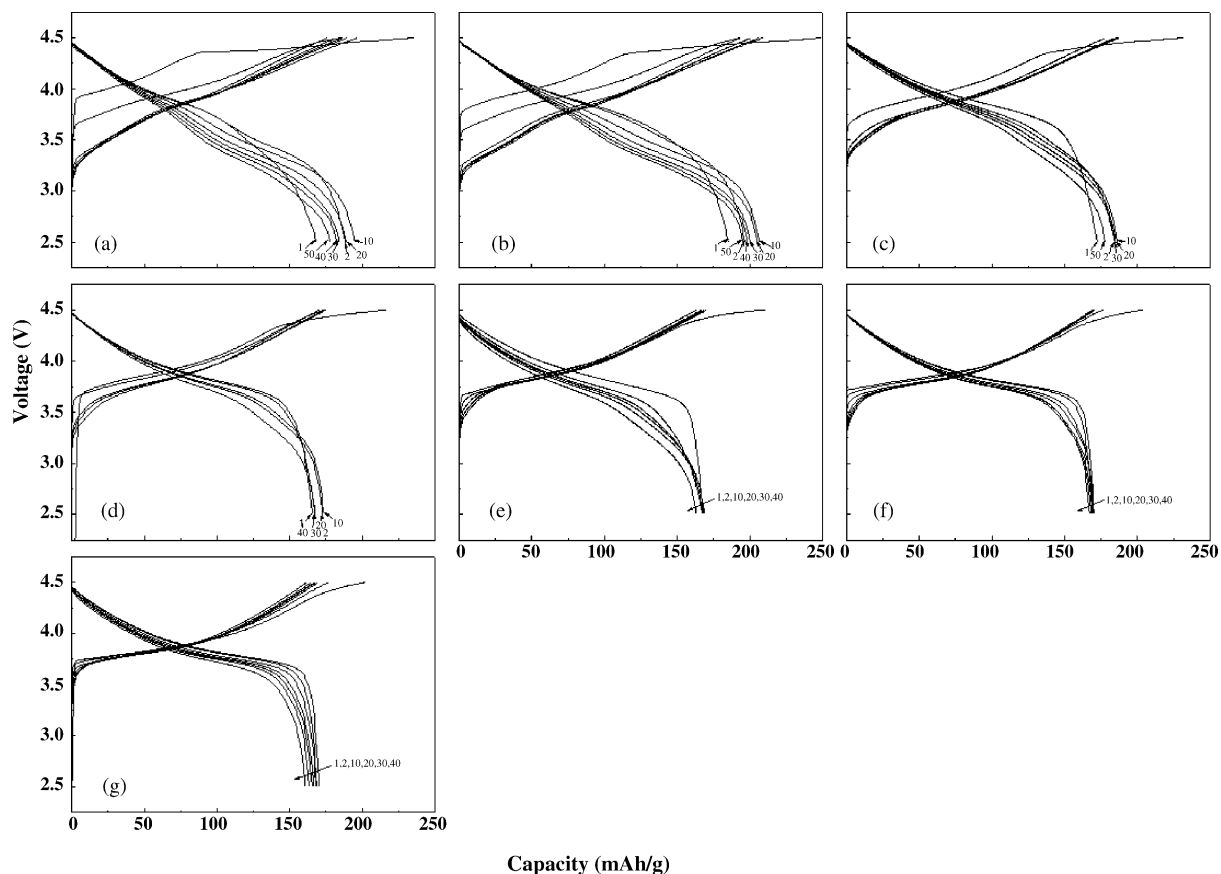


Fig. 4. The charge/discharge curves of Li/LiMO₂ (M = Li_wNi_xCo_yMn_z) cells at a current density of 0.4 mA cm⁻² with a voltage range of 2.5–4.5 V.

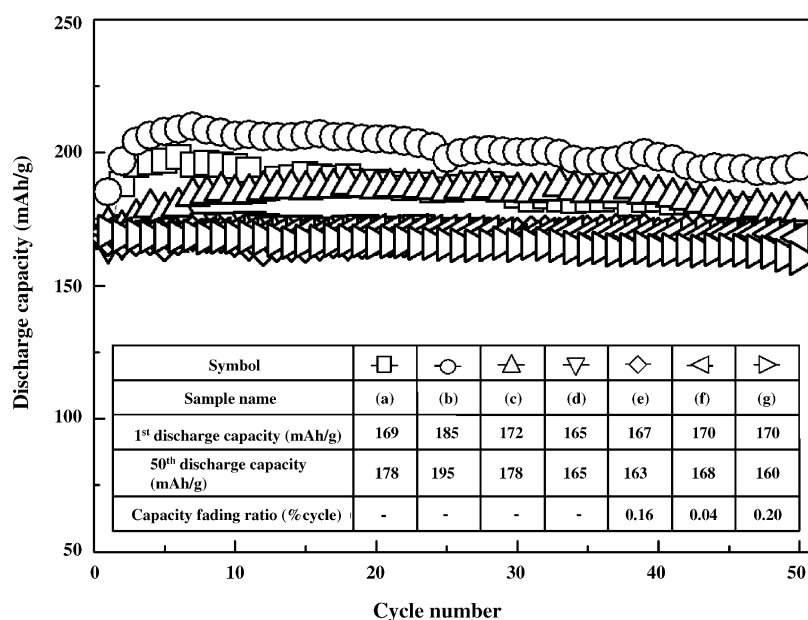


Fig. 5. The cycle number vs. discharge capacity of Li/LiMO₂ (M = Li_wNi_xCo_yMn_z) cells at a current density of 0.4 mA cm⁻² with a voltage range of 2.5–4.5 V.

are derived from the Mn³⁺/Mn⁴⁺ redox couple. For the sample B, the broad peaks are due to the Mn³⁺/Mn⁴⁺ redox couple and are larger than that of sample A, indicating that the discharge capacity of the sample B is higher than that of sample A. A similar observation was reported by Numata et al.

[24] where they studied the cyclic voltammetry behavior of Li(Li_{1-x}Co_{x/3}Mn_{2x/3})O₂. In Fig. 5, it was observed that the samples A–D increase the discharge capacity from the first cycle. In the first charge state, the as-prepared samples maintain the Mn oxidation state of 4+. But the Mn begins to undergo a change

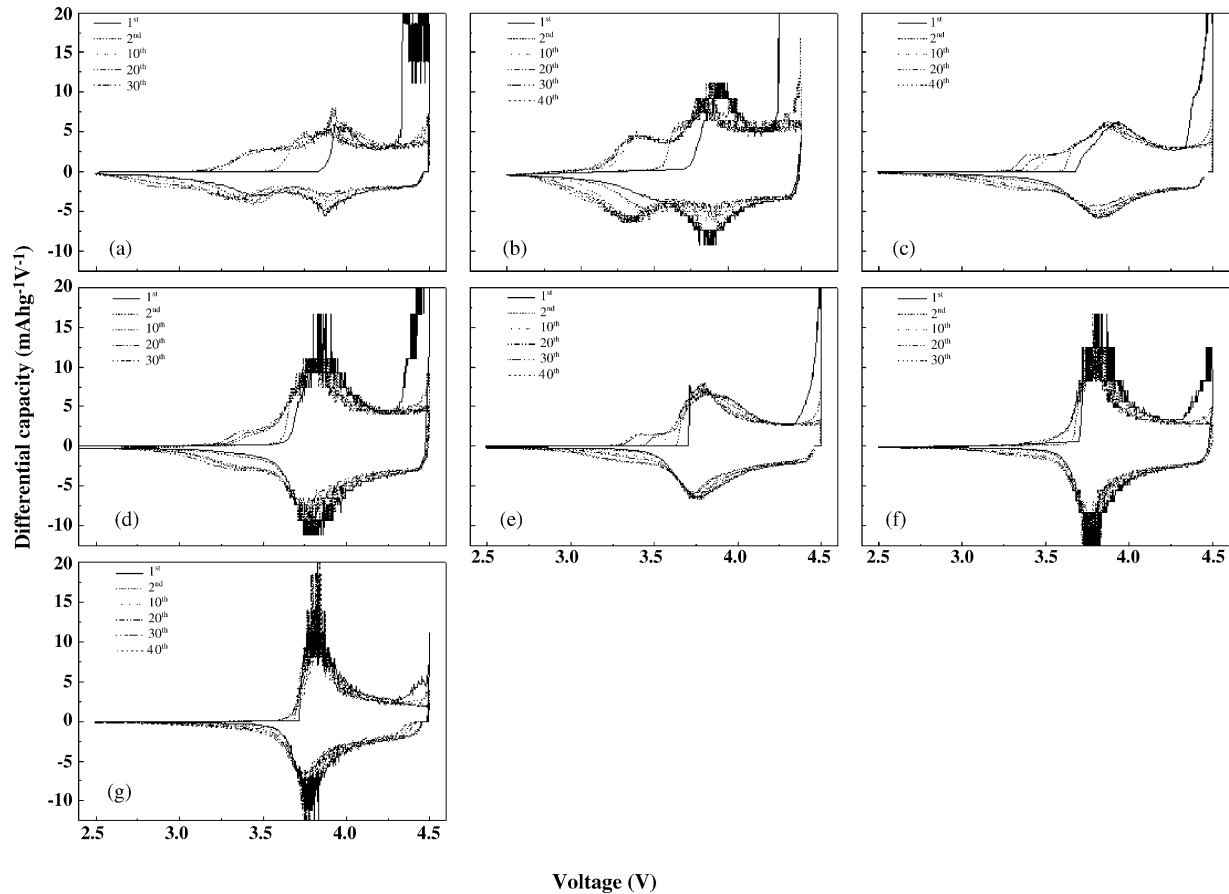


Fig. 6. Voltage vs. differential capacity of Li/LiMO₂ (M = Li_wNi_xCo_yMn_z) cells at a current density of 0.4 mA cm⁻² with a voltage range of 2.5–4.5 V.

in oxidation state due to the irreversible charge capacity which appeared in the first charge state at a high voltage of 4.5 V, resulting in an increase in discharge capacity from the second cycle. The irreversible capacity is ascribed to the extraction of Li ions from the transition metal sites, which generates oxygen vacancies on the sites. This causes an imbalance in the total oxidation state in the transition metal layer, leading to a change in the oxidation state of Mn [5,6]. As the Mn content increases from the samples A–G, the peaks of the Mn³⁺/Mn⁴⁺ redox couple at 3.4–3.5 V gradually disappear. The samples F and G do not show the peaks of the Mn redox couple. Dahn et al. [25] could not find the Mn redox peak for the compound, LiNi_{0.5}Mn_{0.5}O₂ when the dQ/dV was plotted. However, in the present study due to Li₂MnO₃, the Mn redox peaks are degenerated for all samples (A–G) and the redox peaks appear in the dQ/dV plot.

Fig. 7 shows the theoretical discharge capacities of all the synthesized samples. The capacity values were calculated from each redox couple, i.e. Ni²⁺/Ni⁴⁺, Co³⁺/Co⁴⁺, Mn³⁺/Mn⁴⁺, by assuming that these redox couples influence the capacity of each sample. Our calculation was based on the equation reported Zhang et al. [26] who proposed a method to estimate the theoretical capacity of solid solutions. It is seen that the capacity of the sample A (without Ni) is principally determined by the redox couples of Co³⁺/Co⁴⁺ and Mn³⁺/Mn⁴⁺. On the contrary,

in the sample G, the effect of Co and Mn almost vanishes, and Ni becomes a more dominant element in determining the capacity. The content of Mn in the sample G is more than that of the sample A. But the Mn contents of Li₂MnO₃ are less than that of the sample A. So, the theoretical capacity of Mn in Li₂MnO₃

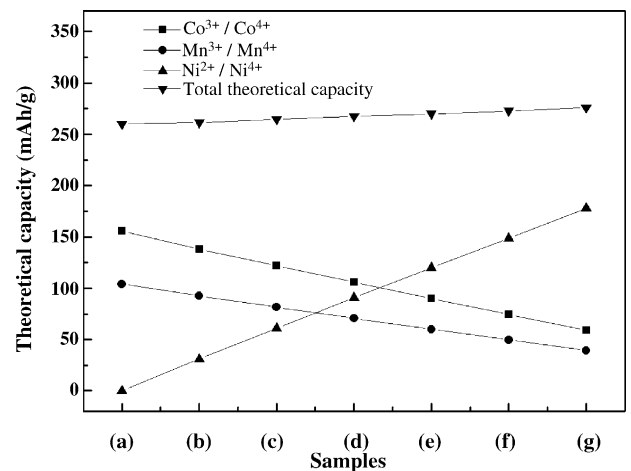


Fig. 7. The theoretical capacity of LiMO₂ (M = Li_wNi_xCo_yMn_z) ($w = 1/15 - 1/6$; $x = 0 - 3/10$; $y = 1/5 - 1/2$; $z = 13/30 - 1/3$; i.e. $w + x + y + z = 1$) vs. the composition of the samples.

is smaller than that of sample A. For the samples C–E, it seems that the charge capacity at the first cycle is due to the overlapping of the $\text{Co}^{3+}/\text{Co}^{4+}$ and $\text{Ni}^{2+}/\text{Ni}^{4+}$ couples. For the samples F and G, it seems that the incorporation of Ni in producing the capacity compensates for the decreased capacity $\text{Co}^{3+}/\text{Co}^{4+}$ and $\text{Mn}^{3+}/\text{Mn}^{4+}$ couple induces. The shape of the discharge curve is more predominant due to the presence of $\text{Ni}^{2+}/\text{Ni}^{4+}$ couple in sample G than that of sample F because the Ni composition is higher in the sample G than in sample F. It is clearly seen that the contents of Co and Mn in the samples play an important role in determining the discharge capacities of the synthesized materials.

4. Conclusions

Layered LiMO_2 ($\text{M} = \text{Li}_w\text{Ni}_x\text{Co}_y\text{Mn}_z$) ($w = 1/15 - 1/6$; $x = 0 - 3/10$; $y = 1/5 - 1/2$; $z = 13/30 - 1/3$; i.e. $w + x + y + z = 1$) solid solutions have been synthesized using the sol–gel method. The contents of Li, Co, Mn and Ni in the transition metal sites were changed to determine the role of these elements in the electrochemical behavior of the solid solutions. The particle sizes of the prepared solid solutions are in the range of 250–500 nm and are semi-spherically shaped. XRD and Raman studies confirmed that the synthesized solid solutions have a typical layered hexagonal phase. The cycling studies revealed that although samples A–D exhibit higher discharge capacities than the samples E–G, the latter samples showed a minimum fade in capacity per cycle.

Acknowledgement

This work was supported by the Core Technology Development Program of the Ministry of Commerce Industry and Energy (MOCIE).

References

- [1] Z.L. Gong, H.S. Liu, X.J. Guo, Z.R. Zhang, Y. Yang, *J. Power Sources* 136 (2004) 139.
- [2] N. Tran, L. Croguennec, C. Jordy, Ph. Biensan, C. Delmas, *Solid-State Ionics* 176 (2005) 1539.
- [3] T. Ohzuku, Y. Makimura, *Chem. Lett.* (2001) 744.
- [4] S.-H. Kang, K. Amine, *J. Power Sources* 124 (2003) 533.
- [5] Ki Soo Park, Myung Hun Cho, Sung Jang Jin, Kee Suk Nahm, *Electrochem. Solid-State Lett.* 7 (2004) A239.
- [6] Ki Soo Park, Myung Hun Cho, Sung Jang Jin, Kee Suk Nahm, *Solid-State Ionics* 171 (2004) 141.
- [7] K. Numata, C. Sakaki, S. Yamanaka, *Solid-State Ionics* 117 (1999) 257.
- [8] J.-H. Kim, C.W. Park, Y.-K. Sun, *Solid-State Ionics* 164 (2003) 43.
- [9] L. Zhang, K. Takada, N. Ohta, L. Wang, T. Sasaki, M. Watanabe, *Mater. Lett.* 58 (2004) 3197.
- [10] Z. Lu, L.Y. Beaulieu, R.A. Donabarger, C.L. Thomas, J.R. Dahn, *J. Electrochem. Soc.* 149 (2002) A778.
- [11] J. Breger, M. Jiang, N. Dupre, Y.S. Meng, Y.S. Horn, G. Ceder, C.P. Grey, *J. Solid-State Chem.* 178 (2005) 2575.
- [12] J.S. Kim, C.S. Johnson, J.T. Vaughey, M.M. Tahckeray, S.A. Hackney, W. Yoon, C.P. Grey, *Chem. Mater.* 16 (2004) 1996.
- [13] Z. Lu, Z. Chen, J.R. Dahn, *Chem. Mater.* 15 (2003) 3214.
- [14] C.M. Julien, M. Massot, *Mater. Sci. Eng. B* 100 (2003) 69.
- [15] C. Julien, M. Massot, C. Perez-Vicente, E. Haro-Poniatowski, G.A. Narzi, A. Rougier, *Mater. Res. Soc. Symp. Proc.* 496 (1998) 415.
- [16] A. Rougier, G.A. Narzi, C. Julien, *Ionics* 3 (1997) 170.
- [17] X. Wu, Yong J. Park, K.S. Ryu, Y.-G. Lee, S. Ho Chang, *Solid-State Ionics* 149 (2004) 145.
- [18] B. Ammundsen, J. Paulsen, I. Davidson, R.S. Liu, C.H. Shen, J.M. Chen, L.Y. Jang, J.F. Lee, *J. Electrochem. Soc.* 149 (2002) A431.
- [19] S. Kikkawa, S. Miyazaki, M. Koizumi, *J. Power Sources* 14 (1985) 231.
- [20] Z. Lu, J.R. Dahn, *J. Electrochem. Soc.* 149 (2002) A815.
- [21] S.S. Shin, Y.K. Sun, K. Amine, *J. Power Sources* 112 (2002) 634.
- [22] S.H. Park, Y.K. Sun, *J. Power Sources* 119–121 (2003) 161.
- [23] J.H. Kim, Y.K. Sun, *J. Power Sources* 119–121 (2003) 166.
- [24] K. Numata, Y. Yamanaka, *Solid-State Ionics* 118 (1999) 117.
- [25] D.D. MacNeil, Z. Lu, J.R. Dahn, *J. Electrochem. Soc.* 149 (2002) A1332.
- [26] L. Zhang, H. Noguchi, M. Yoshio, *J. Power Sources* 110 (2002) 57.